

## Synchronization measures of bursting data: Application to the electrocorticogram of an auditory event-related experiment

Mark A. Kramer,<sup>1</sup> Erik Edwards,<sup>2</sup> Maryam Soltani,<sup>2</sup> Mitchel S. Berger,<sup>3</sup> Robert T. Knight,<sup>2</sup> and Andrew J. Szeri<sup>1,4,\*</sup>

<sup>1</sup>*Program in Applied Science and Technology, University of California, Berkeley, California 94720-1708, USA*

<sup>2</sup>*Department of Psychology and The Helen Wills Neuroscience Institute, University of California, Berkeley, California 94720-1650, USA*

<sup>3</sup>*Department of Neurological Surgery, University of California, San Francisco, California 94143, USA*

<sup>4</sup>*Department of Mechanical Engineering, University of California, Berkeley, California 94720-1740, USA*

(Received 5 November 2003; revised manuscript received 17 February 2004; published 29 July 2004)

Synchronization measures have become an important tool for exploring the relationships between time series. We review three recently proposed nonlinear synchronization measures and expand their definitions in a straightforward way to apply to an ensemble of measurements. We also develop a synchronization measure in which nearest neighbors are determined across the ensemble. We compare these four nonlinear synchronization measures and show that our measure succeeds in physically motivated examples where the other methods fail. We apply the synchronization measure to human electrocorticogram data collected during an auditory event-related potential experiment. The results suggest a crude model of cortical connectivity.

DOI: 10.1103/PhysRevE.70.011914

PACS number(s): 87.19.Nn, 05.45.Tp, 05.45.Xt, 87.19.La

### I. INTRODUCTION

The electrocorticogram (ECoG) is a measure of the electric potential on the cortical surface of the brain. Although of higher spatial resolution than the scalp electroencephalogram (EEG), the ECoG still records the summed activity from millions of individual neurons. In order to better understand the relationships between microscopic neurons and macroscopic electric potential recordings, the human neocortex (roughly the outermost 3 mm of the brain) can be divided into functional units called cortical macrocolumns [1]. Each macrocolumn contains approximately  $10^6$  neurons and  $10^{10}$  synapses, which connect each neuron to neighboring neurons, neighboring macrocolumns, and more distant regions of the brain. Understanding the interactions between cortical macrocolumns, although more tractable than the interactions between individual neurons, is still a demanding problem. Instead, relationships between pairs of electrodes—which record activity summed over cortical macrocolumns—are used to infer relationships between larger regions of the neocortex.

The relationships between two time series recorded simultaneously from different electrodes have been investigated with many techniques. These include measures of linear interdependence, such as cross correlation [2], coherence [3,4], and event-related coherence [5], and more recent measures of nonlinear interdependence, such as mutual information and synchronization [6,7]. Traditional information measures have been shown to depend strongly on the embedding dimension and time delay for short EEG time series [8], although clever, nonstandard techniques may overcome this limitation [9]. Synchronization techniques are useful for the analysis of short time series of noisy data, characteristic of ECoG event-related potential (ERP) measurements.

Various synchronization measures have been developed. These include identical synchronization [10], generalized

synchronization [11], phase synchronization [12], and synchronization techniques robust to noisy data [6,13]. These synchronization measures are generally applied to pairs of time series from a single simulation or experiment. Here we discuss the application of three well-known synchronization measures to an ensemble of repeated measurements, as occurs in the ECoG experiment of interest in the present work. We find that these measures give erroneous results when applied to physically motivated, simulated data. To overcome this limitation, we develop a synchronization measure in which nearest neighbors are determined across the ensemble of measurements, rather than within each individual ensemble member.

This paper is organized as follows. In Sec. II A we restate three well-known synchronization measures and define a new synchronization measure in Sec. II B. In Secs. III and IV we apply these measures to the unidirectionally coupled non-identical Henon map and to model data of bursting oscillatory activity, respectively. We show that only our synchronization measure succeeds in detecting the types of interdependence expected in ECoG ERP experiments. In Sec. V we apply the synchronization measure to actual human ECoG data collected during an auditory ERP experiment and suggest a simple model for the results. Finally, in Sec. VI we summarize the results and present our conclusions.

### II. INTERDEPENDENCE MEASURES

In this section we review three synchronization measures from [6] and [8]. We apply each measure to an ensemble of scalar time series  $s^k[n]$  and  $r^k[n]$ , where the time index  $n = \{1, \dots, n'\}$  and the ensemble index  $k = \{1, \dots, k'\}$ . Specifically, we think of  $s^k[n]$  and  $r^k[n]$  as the value of the electric potential recorded simultaneously at two different electrodes as a function of discrete time  $n$ . The physical time  $t$  is related to the discrete time  $n$  by  $t = n\Delta t + t_0$  where  $t_0$  is the initial time and  $\Delta t$  is the sampling interval. Each ensemble member  $k$  represents a unique realization of the same experiment. The

\*Electronic address: aszeri@me.berkeley.edu

synchronization measure is computed for each ensemble member pair (i.e.,  $s^k[n]$  and  $r^k[n]$  with  $k$  fixed) and the resulting synchronization values are averaged over the entire ensemble.

The ensemble formalism is particularly useful for our application of interest. Electrooculogram measurements often involve the response of the neocortex triggered by a specific stimulus, for example an auditory tone. Typically in the ERP experiments the response to the sensory stimulus is oscillatory, weak, and of short duration ( $n'$  is small). Therefore, an ensemble of ERPs is recorded (with time referenced to the stimulus onset) and various measures are averaged over the ensemble to improve the signal to noise ratio. Physically, ensemble averaging assumes that repetitive applications of the stimulus activate similar pathways in the brain [14]. We therefore expect that the ERP will begin at approximately the same time—say, 100 ms—after each stimulus presentation. We further assume that the response of the neocortex will trace the same dynamics with each stimulus presentation. In what follows we will show how this assumption is useful.

The synchronization measures require that we reconstruct the state space of the system  $\mathbf{x}^k[n] = (s^k[n], s^k[n + \tau], \dots, s^k[n + (d-1)\tau])$  and  $\mathbf{y}^k[n] = (r^k[n], r^k[n + \tau], \dots, r^k[n + (d-1)\tau])$  for each pair of ensemble members [15]. Here  $\tau$  denotes the delay time and  $d$  the embedding dimension, which we assume are the same for both ensembles and all ensemble members. The standard procedures for determining  $\tau$  and  $d$  are demanding;  $\tau$  is often assigned to be the time of the first minimum of the average mutual information, and  $d$  is calculated through a false nearest-neighbor procedure [15]. Both of these calculations are questionable for short data sets of noisy, nonstationary data, which are typical in ECoG ERP experiments. Using [15] as a guide, we considered different values of  $\tau$  and  $d$ , and found stable results.

### A. Current synchronization measures

We now define three synchronization measures in current use and discuss a simple method of ensemble averaging. The first two synchronization measures  $S(\mathbf{x}[n]|\mathbf{y})$  and  $H(\mathbf{x}[n]|\mathbf{y})$  follow from [6]. Denote as  $n_{k,i}$  the time indices of the  $N$  nearest neighbors to the element  $\mathbf{x}^k[n]$  of the  $k$ th member of the ensemble at time  $n$ . We note that  $\mathbf{x}^k[n]$  and its nearest neighbors are all elements of the  $k$ th member of the ensemble. Define the mean-squared Euclidean distance from the element  $\mathbf{x}^k[n]$  to its  $N$  nearest neighbors as

$$R(\mathbf{x}^k[n]) = \frac{1}{N} \sum_{i=1}^N (\mathbf{x}^k[n] - \mathbf{x}^k[n_{k,i}])^2. \quad (1)$$

Note that  $R(\mathbf{x}^k[n])$  is a function of time  $n$  through  $\mathbf{x}^k[n]$ . Similarly, denote the time indices of the nearest neighbors to  $\mathbf{y}^k[n]$  as  $m_{k,i}$  and define

$$R(\mathbf{x}^k[n]|\mathbf{y}) = \frac{1}{N} \sum_{i=1}^N (\mathbf{x}^k[n] - \mathbf{x}^k[m_{k,i}])^2. \quad (2)$$

Here, we calculate the average squared distance from  $\mathbf{x}^k[n]$  to elements in the same ensemble  $k$  using the time indices  $(m_{k,i})$  from ensemble  $\mathbf{y}^k[n]$ . Then we define

$$S(\mathbf{x}^k[n]|\mathbf{y}) = \frac{R(\mathbf{x}^k[n])}{R(\mathbf{x}^k[n]|\mathbf{y})}, \quad (3)$$

which when averaged over ensembles yields

$$S(\mathbf{x}[n]|\mathbf{y}) = \frac{1}{k'} \sum_{k=1}^{k'} \frac{R(\mathbf{x}^k[n])}{R(\mathbf{x}^k[n]|\mathbf{y})}. \quad (4)$$

If the ensembles  $\mathbf{x}$  and  $\mathbf{y}$  are synchronous at time  $n$ , then  $S(\mathbf{x}[n]|\mathbf{y}) \rightarrow 1$ ; if they are independent, then  $S(\mathbf{x}[n]|\mathbf{y}) \sim 0$ . Here  $S(\mathbf{x}[n]|\mathbf{y})$  is the first synchronization measure we consider. We note that a variation of this measure, intended to account for noisy data, can be found in [13].

Next we define the mean-squared distance from  $\mathbf{x}^k[n]$  to every time point in the ensemble  $k$ :

$$\bar{R}(\mathbf{x}^k[n]) = \frac{1}{P-1} \sum_{p=1}^P (\mathbf{x}^k[n] - \mathbf{x}^k[p])^2, \quad (5)$$

where  $P = n' - (d-1)\tau$ . Then, from [6], define

$$H(\mathbf{x}^k[n]|\mathbf{y}) = \ln \frac{\bar{R}(\mathbf{x}^k[n])}{R(\mathbf{x}^k[n]|\mathbf{y})}, \quad (6)$$

which we average over the ensembles to obtain

$$H(\mathbf{x}[n]|\mathbf{y}) = \frac{1}{k'} \sum_{k=1}^{k'} \ln \frac{\bar{R}(\mathbf{x}^k[n])}{R(\mathbf{x}^k[n]|\mathbf{y})} \quad (7)$$

as the second synchronization measure. Finally, in [8] a (nearly) normalized synchronization measure is proposed which in our notation becomes

$$N(\mathbf{x}[n]|\mathbf{y}) = \frac{1}{k'} \sum_{k=1}^{k'} \frac{\bar{R}(\mathbf{x}^k[n]) - R(\mathbf{x}^k[n]|\mathbf{y})}{\bar{R}(\mathbf{x}^k[n])}. \quad (8)$$

Note that  $N(\mathbf{x}[n]|\mathbf{y})$  is also ensemble averaged. Equations (4), (7), and (8) are well-known synchronization measures and are included here with a simple ensemble averaging scheme. We apply each of these measures to simulated data in Secs. III and IV.

Before introducing our synchronization measure, we illustrate how the nearest neighbors are chosen in the synchronization measures  $S(\mathbf{x}[n]|\mathbf{y})$ ,  $H(\mathbf{x}[n]|\mathbf{y})$ , and  $N(\mathbf{x}[n]|\mathbf{y})$ . In Fig. 1(a) we show a typical ensemble member  $s^k[n]$  for the ECoG ERP experiment discussed in detail in Sec. V. The stimulus occurs at time  $t=0$  ms. Note that before the stimulus the measured voltage fluctuates between  $\pm 20$  mV, while after the stimulus an oscillatory burst occurs between  $t=30$  ms and  $t=160$  ms. After the oscillatory burst, the voltage returns to its prestimulus range.

We now discuss the procedure for finding nearest neighbors to a point within the oscillatory burst. For illustrative purposes, we embedded the ensemble member  $s^k[n]$  using  $d=3$  and  $\tau=10$ . We show this embedding,  $\mathbf{x}^k[n]$ , in Fig. 1(b). The point marked with an asterisk in Figs. 1(a) and 1(b) is the same and corresponds to a point in the oscillatory burst of  $s^k[n]$ . Denote the time index of this point as  $n^*$ . In Fig. 1(c) we show the local neighborhood of  $\mathbf{x}^k[n^*]$ , and we mark

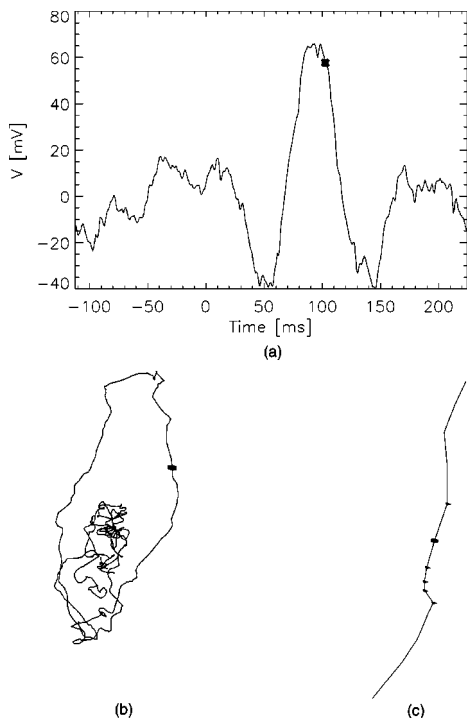


FIG. 1. (a) The electric potential of one ensemble member recorded by one electrode in the ECoG ERP experiment. The stimulus occurs at  $t=0$  ms. Note the oscillatory burst between 30 ms and 160 ms. The asterisk marks a point on the oscillatory burst. (b) The embedding of the times series in (a). We chose  $d=3$  and  $\tau=10$  for illustrative purposes. The asterisk in this figure corresponds to the asterisk in (a). (c) The local neighborhood of the point marked with an asterisk in (b). The five nearest neighbors to this point are marked by triangles. The nearest neighbors are temporally proximal to the fiducial point because the data set is short.

the five nearest neighbors to  $\mathbf{x}^k[n^*]$  with triangles. It is clear from Figs. 1(b) and 1(c) that the nearest neighbors to  $\mathbf{x}^k[n^*]$  lie immediately along the trajectory passing through  $\mathbf{x}^k[n^*]$ . By excluding nearest neighbors within a local temporal window near  $\mathbf{x}^k[n^*]$ , we only succeed in selecting neighbors further along this isolated trajectory. For this case, the trajectory of a single ensemble member does not cover anything like an attractor in the embedding space. Therefore neighbors along the oscillatory burst must be defined with care. We show in what follows that by considering neighbors across the ensemble of measurements, we can—in this case—construct a more representative picture of the underlying dynamics when the data are available only in short data sets.

### B. Synchronization measure

The method we propose is similar to those discussed in [6] and [8]. But for the our synchronization measure, nearest neighbors are chosen from across the ensemble of measurements, rather than from within each individual ensemble member. To illustrate this idea, we show in Fig. 2(a) ten ensembles embedded using  $d=3$  and  $\tau=10$ . The darkest curve in the figure is the single ensemble member shown in Fig. 1(b). Now the element of ensemble  $k$  at time  $t=n^*$ ,

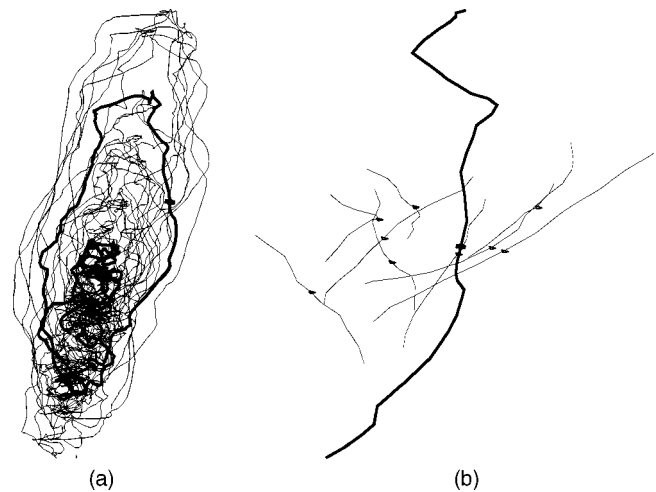


FIG. 2. (a) Ten ensemble members embedded using  $d=3$  and  $\tau=10$ . The thickest curve is the ensemble member shown in Figs. 1(a) and 1(b). The point  $\mathbf{x}^k[n^*]$  is marked with an asterisk. (b) The local neighborhood of the point  $\mathbf{x}^k[n^*]$ . The thickest curve is the trajectory of  $\mathbf{x}^k[n]$ . The point  $\mathbf{x}^k[n^*]$  is marked with an asterisk. The thin curves are trajectories of nine other ensemble members. The nearest ensemble neighbors are marked with triangles.

$\mathbf{x}^k[n^*]$ , has a nearest neighbor in each ensemble  $l \neq k$ . Notice we do not include the nearest neighbor to  $\mathbf{x}^k[n^*]$  in ensemble  $k$ . Finding a single nearest neighbor to  $\mathbf{x}^k[n^*]$  in each ensemble  $l \neq k$ , rather than throughout a single time series, avoids the complications associated with serial correlations of the data from short data sets. In general we denote the time index of the nearest neighbor to  $\mathbf{x}^k[n]$  in ensemble  $l$  as  $n_{k,l}$  and call this set of neighbors the *nearest ensemble neighbors* to  $\mathbf{x}^k[n]$ . In Fig. 2(b), we show the local neighborhood of the point  $\mathbf{x}^k[n^*]$ ; we mark the point  $\mathbf{x}^k[n^*]$  with an asterisk and the ten nearest ensemble neighbors to this point with triangles. Here the neighbors are chosen from across the ensemble of measurements, rather than within each individual ensemble member. Because we have assumed that the trajectory of each ensemble member follows similar dynamics, this method of determining neighbors is justified.

Now we define the synchronization measure. As in Sec. II A we reconstruct the state spaces of the time series  $s^k[n]$  and  $r^k[n]$  to create  $\mathbf{x}^k[n]$  and  $\mathbf{y}^k[n]$ , respectively. For each time point  $n$  of every ensemble member  $k$  we calculate the mean Euclidean distance from  $\mathbf{x}^k[n]$  to its  $k'-1$  nearest ensemble neighbors:

$$D(\mathbf{x}^k[n]) = \frac{1}{k'-1} \sum_{\substack{l=1 \\ l \neq k}}^{k'} \|\mathbf{x}^k[n] - \mathbf{x}^l[n_{k,l}]\|. \quad (9)$$

Here  $\|\cdot\|$  denotes the Euclidean distance, and the  $n_{k,l}$  are the time indices of the nearest ensemble neighbors to  $\mathbf{x}^k[n]$ . We also calculate the standard deviation  $\sigma_D(\mathbf{x}^k[n])$  of the mean distance in Eq. (9). Similarly, denote the time indices of the nearest ensemble neighbors to  $\mathbf{y}^k[n]$  as  $m_{k,l}$ . Then compute the following:

$$T(\mathbf{x}^k[n]|\mathbf{y}) = \frac{1}{k' - 1} \sum_{\substack{l=1 \\ l \neq k}}^{k'} \Theta(D(\mathbf{x}^k[n]) + \sigma_D(\mathbf{x}^k[n]) - \|\mathbf{x}^k[n] - \mathbf{x}^l[m_{k,l}]\|), \quad (10)$$

where  $\Theta(\cdot)$  is the Heaviside step function. In Eq. (10) we determine the distance from  $\mathbf{x}^k[n]$  to each  $\mathbf{x}^l[m_{k,l}]$ . If this distance is less than  $D(\mathbf{x}^k[n]) + \sigma_D(\mathbf{x}^k[n])$  (i.e., the average distance from  $\mathbf{x}^k[n]$  to its nearest ensemble neighbors plus one standard deviation), then  $\mathbf{y}^l[m_{k,l}]$  is a neighbor of  $\mathbf{y}^k[n]$  and  $\mathbf{x}^l[m_{k,l}]$  is a neighbor of  $\mathbf{x}^k[n]$ . Thus, a neighbor of  $\mathbf{x}^k[n]$  and  $\mathbf{y}^k[n]$  shares the same ensemble  $l$  and time index  $m_{k,l}$ . Call this neighbor a *shared neighbor* of  $\mathbf{x}^k[n]$  and  $\mathbf{y}^k[n]$ . By summing the number of shared neighbors between  $\mathbf{x}^k[n]$  and  $\mathbf{y}^k[n]$  and dividing by the total number of possible neighbors—the number of ensemble members  $k'$  minus one—we measure the synchronization between the two time series at time  $n$  in Eq. (10). We average Eq. (10) over the ensemble of measurements to yield

$$T(\mathbf{x}[n]|\mathbf{y}) = \frac{1}{k'} \sum_{k=1}^{k'} T(\mathbf{x}^k[n]|\mathbf{y}). \quad (11)$$

The measure (11) differs from the synchronization measures in Eqs. (4), (7), and (8). In Eq. (11) we compute neighbors from across the ensemble of measurements and determine the fraction of shared neighbors between ensembles  $\mathbf{y}$  and  $\mathbf{x}$ . If for some time index  $n$  this fraction approaches 1.0, then we say that the synchronization between the two ensembles is strong at time  $n$ . If this fraction approaches 0.0, then we say that the synchronization is weak. We include the standard deviation  $\sigma_D(\mathbf{x}^k[n])$  in Eq. (10) to extend the radius of the neighborhood around  $\mathbf{x}^k[n]$ ; a stricter measure of synchronization results if we exclude this term. The interpretation of Eq. (11) is somewhat clearer than the ratio of mean-squared distances utilized in the synchronization methods of Sec. II A. We show in Sec. IV A that the ratio of mean-squared distances can be misleading in certain types of examples.

All of the measures we have discussed determine the ensemble-averaged synchronization between ensembles  $\mathbf{x}$  and  $\mathbf{y}$  at a specific time  $n$ . In some applications—ECoG experiments, for example—it may be important to investigate time-delayed synchronization. An idea along these lines was mentioned in [6]. In words, we would like to compare the synchronization between  $\mathbf{x}^k[n]$  and  $\mathbf{y}^k[m]$  when  $n \neq m$ ; i.e., we would like to know whether  $\mathbf{x}^k[n]$  at time  $n$  is related to  $\mathbf{y}^k[m]$  at time  $m$ . To do so, we determine the time indices  $m_{k,l}$  of the nearest ensemble neighbors to  $\mathbf{y}^k[n]$ . We then compute the distance between  $\mathbf{x}^k[n]$  and  $\mathbf{x}^l[m_{k,l}]$  for each  $l \neq k$  and record the number of these points that lie close to  $\mathbf{x}^k[n]$ , as in Eq. (10). Now, we shift the time indices  $m_{k,l}$  by an integer  $\eta$ . We then compute the distance between  $\mathbf{x}^k[n + \eta]$  and  $\mathbf{x}^l[m_{k,l} + \eta]$  for each  $l \neq k$  and record the number of these points that lie close to  $\mathbf{x}^k[n + \eta]$ . Here we are comparing  $\mathbf{x}^k[n + \eta]$  at time  $(n + \eta)$  to the time-shifted nearest ensemble neighbors of  $\mathbf{y}^k[n]$  at time  $n$ . Equation (10) is easily extended to include time-shifted synchronization

$$T(\mathbf{x}^k[n, \eta]|\mathbf{y}) = \frac{1}{k' - 1} \sum_{\substack{l=1 \\ l \neq k}}^{k'} \Theta(D(\mathbf{x}^k[n + \eta]) + \sigma_D(\mathbf{x}^k[n + \eta]) - \|\mathbf{x}^k[n + \eta] - \mathbf{x}^l[m_{k,l} + \eta]\|), \quad (12)$$

where  $\eta$  is an integer time shift. When the distance between  $\mathbf{x}^k[n + \eta]$  and  $\mathbf{x}^l[m_{k,l} + \eta]$  is less than  $D(\mathbf{x}^k[n + \eta]) + \sigma_D(\mathbf{x}^k[n + \eta])$  for all  $l \neq k$ ,  $T(\mathbf{x}^k[n, \eta]|\mathbf{y}) = 1.0$ . It is important to keep in mind that the  $m_{k,l}$  are still based on  $\mathbf{y}^k[n]$ , although this is lost in the notation of Eq. (12). The time shifting scheme is essentially equivalent to delaying the ensembles before applying the measure defined in Eq. (11). We average Eq. (12) over the ensemble to obtain

$$T(\mathbf{x}[n, \eta]|\mathbf{y}) = \frac{1}{k'} \sum_{k=1}^{k'} T(\mathbf{x}^k[n, \eta]|\mathbf{y}). \quad (13)$$

Equation (13) is the time-shifted, ensemble-averaged synchronization between ensembles  $\mathbf{x}$  and  $\mathbf{y}$ . Any of the synchronization measures in Sec. II A could have been modified to include time shifts, but we chose only to consider Eq. (13). We note that  $T(\mathbf{x}^k[n, \eta]|\mathbf{y})$  and  $T(\mathbf{y}^k[n, \eta]|\mathbf{x})$  measure different quantities; in the former neighborhoods of  $\mathbf{y}$  are examined in  $\mathbf{x}$ , while in the latter neighborhoods in  $\mathbf{x}$  are examined in  $\mathbf{y}$ . Determining the driver-response relationship from the asymmetry of these two synchronization measurements is not obvious. We refer the interested reader to [6] and [7].

### III. SIMULATED DATA: HENON MAP

To show that the ensemble formalism proposed in Secs. II A and II B creates useful measures of synchronization, we apply the four synchronization measures to the standard example of the unidirectionally coupled nonidentical Henon map [13]:

$$r^k[n] = 1.4 - r^k[n-1]^2 + 0.3r^k[n-2],$$

$$s^k[n] = 1.4 - \{\kappa[n]r^k[n-1] + (1 - \kappa[n])s^k[n-1]\}s^k[n-1] + 0.1s^k[n-2]. \quad (14)$$

Here, the ensemble members differ only in the initial values of  $s^k[n]$  and  $r^k[n]$ , which are chosen randomly but avoid the fixed points of the system. The coupling strength  $\kappa[n]$  was assigned the value 0.9 (strong coupling) when  $100 < n < 150$  and 0.0 (no coupling) otherwise. We expect the synchronization measures to detect the interdependence between the ensemble members  $s^k[n]$  and  $r^k[n]$  only when the coupling is strong (i.e., when  $100 < n < 150$ ). For this simulation we fixed the number of ensemble members  $k'$  to 20 and chose  $\tau=1$ ,  $d=3$  to reconstruct the state-space vectors  $\mathbf{x}^k[n]$  and  $\mathbf{y}^k[n]$  from  $s^k[n]$  and  $r^k[n]$ , respectively. For the synchronization measures in Sec. II A, each ensemble member was scaled to have zero mean and unit variance. In Fig. 3(a) the synchronization measures  $S(\mathbf{x}[n]|\mathbf{y})$  (dashed line),  $H(\mathbf{x}[n]|\mathbf{y})$  (dotted line), and  $N(\mathbf{x}[n]|\mathbf{y})$  (solid line) are shown. It is clear that all three measures increase during the interval of nonlin-

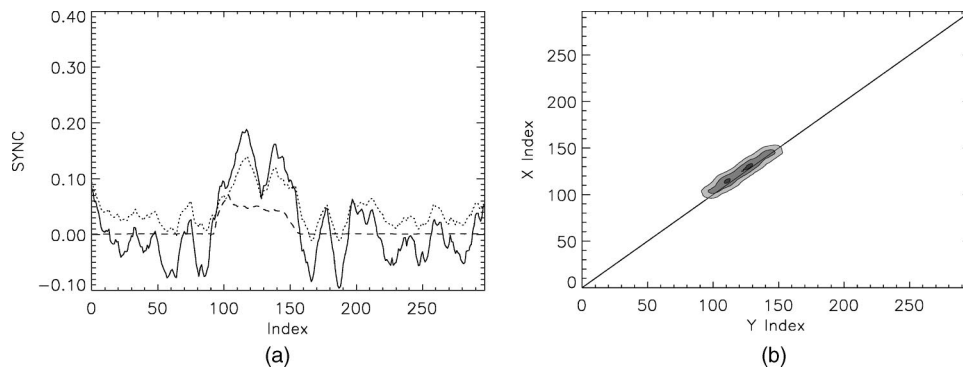


FIG. 3. Synchronization measures applied to the unidirectionally coupled nonidentical Henon map. (a) Three synchronization measures:  $S(\mathbf{x}[n]|\mathbf{y})$  (dashed line),  $H(\mathbf{x}[n]|\mathbf{y})$  (dotted line), and  $N(\mathbf{x}[n]|\mathbf{y})$  (solid line). All of the measures are smoothed over a window of size 11 at each time point. All three measures increase during the interval of nonlinear coupling ( $100 < n < 150$ ) between the chaotic time series. (b) The time-shifted synchronization measure  $T(\mathbf{x}[n, \eta]|\mathbf{y})$  smoothed over a two-dimensional window of size 11 at each time point. Note that the planar axes show time along ensembles  $\mathbf{y}$  and  $\mathbf{x}$ , respectively. In the contour plot, there are five evenly spaced contour levels, ranging from 0.0 (white) to 0.08 (black). Unless defined otherwise, all  $T(\mathbf{x}[n, \eta]|\mathbf{y})$  figures follow this gray-scale scheme. The diagonal line in the figure corresponds to the location of zero time lag. The contour plot shows synchronization occurs with time shift  $\eta=0$  during the time interval  $100 < n < 150$ .

ear coupling between the two ensembles:  $100 < n < 150$ . In Fig. 3(b) we plot the time-shifted synchronization measure  $T(\mathbf{x}[n, \eta]|\mathbf{y})$ . Again, the nonlinear coupling between the two ensembles is clear and appears as the thin diagonal band in the contour plot. From the location of the band in Fig. 3(b) we conclude that ensembles  $\mathbf{x}^k[n]$  and  $\mathbf{y}^k[n]$  are synchronous when  $100 < n < 150$ ; i.e., the two are coupled with no time shift. The reader may wonder why the values of  $T(\mathbf{x}[n, \eta]|\mathbf{y})$  are so small; in Fig. 3(b) the contour levels range from 0.0 (white) to 0.08 (black). This follows from the rather tight definition we have adopted in Eq. (12) for the neighborhood of  $\mathbf{x}^k[n]$ . It may be profitable to relax this definition for very noisy data.

**IV. SIMULATED DATA: OSCILLATORY BURSTS**

In this section we apply the synchronization measures of Sec. II to simulated data. The simulated data are motivated by observed ECoG ERP time series in which weak bursts of oscillatory activity often occur. For example, an auditory stimulus may evoke a 10-Hz burst in one cortical electrode, followed by a 40-Hz burst in another cortical electrode. See [16] for a further discussion. Our goal is to determine which methods accurately detect this specific type of interdependence. We show in the examples that only  $T(\mathbf{x}[n, \eta]|\mathbf{y})$  succeeds in detecting interdependent bursts of oscillatory activity occurring between two ensembles. For all of the examples in this section, we set the total number of ensemble members to 20 ( $k'=20$ ) and let  $n$  represent the physical time, where the sampling interval  $\Delta n = \Delta t$  is 1 ms.

**A. Bursting data versus noise**

We start by considering the case where the two ensembles of time series measurements  $s^k[n]$  and  $r^k[n]$  are unrelated. Specifically, we simulate the case where one cortical electrode measures a response to a stimulus while the other cortical electrode does not. One would expect that all of the

synchronization measures will detect no interdependence between these two ensembles of measurements. However, we show that the measure  $S(\mathbf{x}[n]|\mathbf{y})$  erroneously detects synchronization between the ensembles and explain why this occurs.

We construct  $s^k[n]$  such that each ensemble member consists of identical, weak bursts of oscillatory behavior when  $100 \text{ ms} < n < 150 \text{ ms}$ . Each ensemble member is further constructed from 200 sinusoids, where each sinusoid is assigned a random uniformly distributed frequency (from 0 to 100 Hz) and random uniformly distributed phase (from  $-\pi$  to  $\pi$ ). We scale this sum of 200 sinusoids such that the ratio of the oscillatory burst amplitude to the amplitude of the summed sinusoids is approximately 2. We denote this ratio of amplitudes the signal-to-noise ratio (SNR). Here the oscillatory bursts represent evoked responses while the sinusoids act as noise. We shall refer to this type of noise as *sinusoidal noise*. The ensemble members of  $r^k[n]$  consist only of sinusoidal noise (i.e., these ensemble members possess no evoked responses.) We show an example of the individual ensemble members in Fig. 4(a). Here the weak evoked response of  $s^k[n]$  (solid line) is mostly hidden by the noise. After averaging the time series over the ensembles, the evoked response in ensemble  $s$  and lack of response in ensemble  $r$  become apparent in Fig. 4(b).

To calculate the synchronization between the two ensembles we chose  $\tau=1$  and  $d=10$  to reconstruct the state-space vectors  $\mathbf{x}^k[n]$  and  $\mathbf{y}^k[n]$  from  $s^k[n]$  and  $r^k[n]$ , respectively. We expect all of the synchronization measures will detect no synchronization between the two ensembles. In Fig. 4(c) we plot the synchronization measures  $S(\mathbf{x}[n]|\mathbf{y})$  (dashed line),  $H(\mathbf{x}[n]|\mathbf{y})$  (dotted line), and  $N(\mathbf{x}[n]|\mathbf{y})$  (solid line). Both  $H(\mathbf{x}[n]|\mathbf{y})$  and  $N(\mathbf{x}[n]|\mathbf{y})$  fluctuate between 0.2 and 0.55 but possess no obvious structure suggestive of a change in synchronization between the two ensembles.  $S(\mathbf{x}[n]|\mathbf{y})$ , though, suggests a doubling (from  $\sim 0.1$  to  $\sim 0.25$ ) in synchronization between the two ensembles during the time of the oscillatory burst in  $s^k[n]$ . This is caused

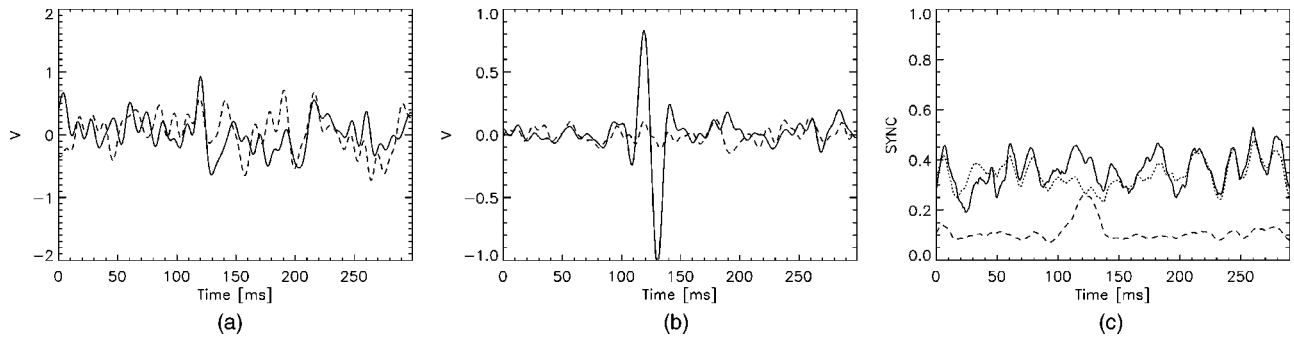


FIG. 4. Nonlinear synchronization measures applied to oscillatory bursting data versus noisy data. (a) A typical ensemble member from the oscillatory bursting data  $s^k[n]$  (solid line) and the noisy data  $r^k[n]$  (dashed line). The weak oscillatory response in  $s^k[n]$  between 100 ms and 150 ms is hidden in the noise. (b) The ensemble-averaged ERPs of ensemble  $s$  (solid) and ensemble  $r$  (dashed). The oscillatory response in ensemble  $s$  for  $100 \text{ ms} < n < 150 \text{ ms}$  is apparent. (c) Three synchronization measures:  $S(\mathbf{x}[n]|\mathbf{y})$  (dashed line),  $H(\mathbf{x}[n]|\mathbf{y})$  (dotted line), and  $N(\mathbf{x}[n]|\mathbf{y})$  (solid line). All three measures are smoothed over a window of size 11 ms at each time point. Both  $H(\mathbf{x}[n]|\mathbf{y})$  and  $N(\mathbf{x}[n]|\mathbf{y})$  fluctuate between 0.2 and 0.55 over the entire time interval and suggest no obvious synchronization between the ensembles, as expected.  $S(\mathbf{x}[n]|\mathbf{y})$  increases during the interval  $100 \text{ ms} < n < 150 \text{ ms}$  and therefore suggests an increased synchronization between the ensembles during this interval. This incorrect interpretation is a consequence of the increase in  $R(\mathbf{x}^k[n])$  during the oscillatory burst, as explained in the text.

by the numerator of Eq. (3),  $R(\mathbf{x}^k[n])$ , which increases during the oscillatory burst due to the increased distance from  $\mathbf{x}^k[n]$  to its nearest neighbors during this interval. The denominator of Eq. (3),  $R(\mathbf{x}^k[n]|\mathbf{y})$ , also increases during the interval of oscillatory behavior, though not enough to compensate for the increase in  $R(\mathbf{x}^k[n])$ . Thus, the increase in  $S(\mathbf{x}[n]|\mathbf{y})$  for this example is due to an increase in  $R(\mathbf{x}^k[n])$ , not an increase in the synchronization between the two ensembles. The synchronization measure  $T(\mathbf{x}[n], \eta)|\mathbf{y}$  (not shown) detects no interdependence between the two ensembles, as expected. In the next example we will not consider  $S(\mathbf{x}[n]|\mathbf{y})$ .

### B. Simultaneous bursts

We now consider the case where both ensembles respond to the stimulus, but in different ways. In this example, a high-frequency burst of oscillatory activity occurs in  $s^k[n]$  and a simultaneous lower-frequency burst of oscillatory activity occurs in  $r^k[n]$  for  $100 \text{ ms} < n < 150 \text{ ms}$  and each  $k$ . Sinusoidal noise is added to each  $s^k[n]$  and  $r^k[n]$  such that

the SNR is approximately 2. A typical ensemble member pair ( $s^k[n]$  solid,  $r^k[n]$  dashed) is shown in Fig. 5(a). The individual ensemble members in Fig. 5(a) do not reveal the structure of the ERP, which is mostly hidden by the noise. Only after averaging an ensemble of these time series do the ERPs become apparent in Fig. 5(b). From the ensemble-averaged data, we conclude that both ensembles possess a nontrivial response to the stimulus. We expect the synchronization measures will detect this type of relationship, in which both ensembles respond to the stimulus simultaneously, although at different frequencies.

To compute the synchronization between ensembles  $s$  and  $r$ , we set  $\tau=1$  and  $d=10$  to reconstruct the state-space vectors  $\mathbf{x}^k[n]$  and  $\mathbf{y}^k[n]$  from  $s^k[n]$  and  $r^k[n]$ , respectively. In Fig. 5(c) we plot  $H(\mathbf{x}[n]|\mathbf{y})$  (dotted line) and  $N(\mathbf{x}[n]|\mathbf{y})$  (solid line). Both results fluctuate throughout the entire time interval. Neither measure accurately captures the interval of synchronization between the two ensembles. We show  $T(\mathbf{x}[n], \eta)|\mathbf{y}$  for this example in Fig. 6. It clearly detects the interdependence between  $s^k[n]$  and  $r^k[n]$  when 100 ms

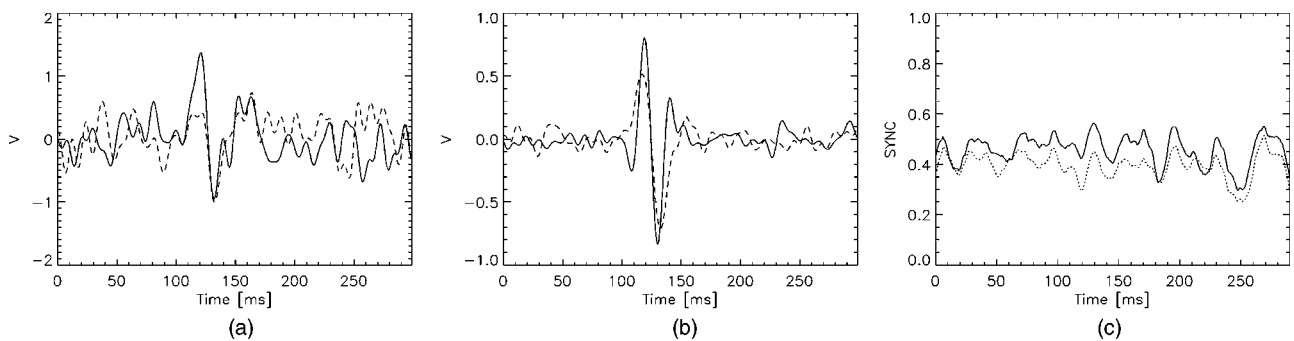


FIG. 5. (a) A typical ensemble member pair from the oscillatory bursting data:  $s^k[n]$  (solid line) and  $r^k[n]$  (dashed line). The weak oscillatory responses of both time series are mostly hidden in the noise. (b) The ensemble-averaged ERPs of  $s^k[n]$  (solid line) and  $r^k[n]$  (dashed line). The oscillatory bursts, hidden in the pair of (a), are revealed here in the ensemble averaged ERPs. (c) Two synchronization measures:  $H(\mathbf{x}[n]|\mathbf{y})$  (dotted line) and  $N(\mathbf{x}[n]|\mathbf{y})$  (solid line), smoothed over a window of size 11 ms at each time point. Neither  $H(\mathbf{x}[n]|\mathbf{y})$  nor  $N(\mathbf{x}[n]|\mathbf{y})$  accurately captures the synchronization between the two ensemble for  $100 \text{ ms} < n < 150 \text{ ms}$ .

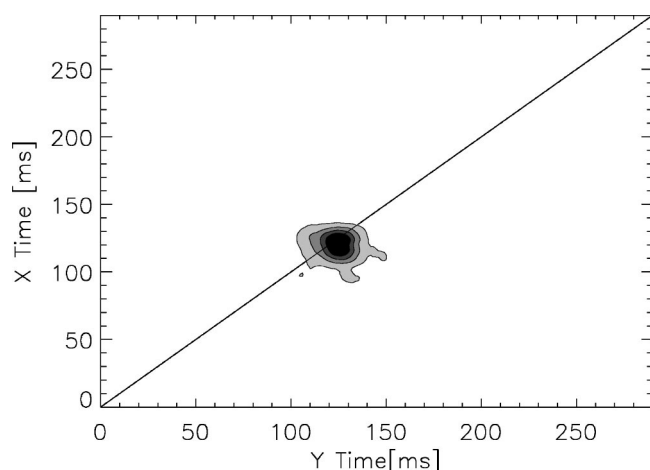


FIG. 6. The time-shifted synchronization  $T(\mathbf{x}[n, \eta]|\mathbf{y})$  applied to the ensemble of oscillatory bursting data of Fig. 5.  $T(\mathbf{x}[n, \eta]|\mathbf{y})$  was smoothed over a two-dimensional window of size 11 at each time point. The solid diagonal line corresponds to the location of zero time lag. This measure detects the synchronization between the two ensembles for  $100 \text{ ms} < n < 150 \text{ ms}$ .

$< n < 150 \text{ ms}$ . Of the three synchronization measures applied in this example, only  $T(\mathbf{x}[n, \eta]|\mathbf{y})$  detects the interdependence between the two ensembles. In experimental data, we expect stimuli will evoke responses in different cortical locations at different frequencies. Therefore, we will only use the synchronization measure  $T(\mathbf{x}[n, \eta]|\mathbf{y})$  in our analysis of experimental ECoG ERP data, discussed in Sec. V.

We now summarize the results of our computer simulations. We have shown in Sec. III that the synchronization measures  $S(\mathbf{x}[n]|\mathbf{y})$ ,  $H(\mathbf{x}[n]|\mathbf{y})$ , and  $N(\mathbf{x}[n]|\mathbf{y})$ , as well as our synchronization measure  $T(\mathbf{x}[n, \eta]|\mathbf{y})$ , detect the nonlinear interdependence between an ensemble of measurements constructed from coupled nonlinear Henon maps. In Sec. IV A we showed that  $S(\mathbf{x}[n]|\mathbf{y})$  erroneously detects synchronization between two unrelated ensembles in one of which oscillatory bursts occur. In Sec. IV B we showed that  $H(\mathbf{x}[n]|\mathbf{y})$  and  $N(\mathbf{x}[n]|\mathbf{y})$  fail to detect interdependence between two related ensembles in which bursts of oscillatory activity occur. Our measure  $T(\mathbf{x}[n, \eta]|\mathbf{y})$  is the only measure to behave correctly in the three examples we considered.

We do not wish to suggest that  $S(\mathbf{x}[n]|\mathbf{y})$ ,  $H(\mathbf{x}[n]|\mathbf{y})$ , and  $N(\mathbf{x}[n]|\mathbf{y})$  are poor measures of synchronization. The references in Sec. I have shown the utility of these synchronization methods applied to a variety of simulated and experimental data. Instead, we suggest that these measures are not useful for the particular time series of interest, in which oscillatory bursts of activity occur in ensembles of short data sets. In the next section, we apply  $T(\mathbf{x}[n, \eta]|\mathbf{y})$  to the time series of interest: an ensemble of measurements collected in an ECoG ERP experiment.

## V. APPLICATION: ECoG ERP

Having developed the synchronization measure  $T(\mathbf{x}[n, \eta]|\mathbf{y})$  in Sec. II B and applied it to simulated data in Secs. III and IV, we now apply it to data from an ECoG ERP

experiment. The ECoG data were recorded from an awake patient undergoing neurosurgery for tumor removal. The recordings were done in accordance with UCSF human subjects requirements and patient consent was obtained. Seven carbon ball electrodes (just under 3 mm in diameter) were placed on the left hemisphere around the posterior extent of the Sylvian fissure, near the known position of primary and secondary auditory cortices. Two epidural electrodes served as reference and ground for the differential amplifiers. The analog signals were bandpass filtered in the amplifier between 0.1 and 250 Hz, amplified by  $10^4$ , and digitized at a sampling rate of 2003 Hz with 16-bit resolution. The data were subsequently high-pass filtered above 2.3 Hz using a symmetrical finite-response filter and all epochs with detectable artifact were removed.

The stimuli consisted of short duration (180 ms) tones occurring at two different frequencies. During the experiment, the patient passively heard three 210-s blocks of tones while watching a slide show. In the first and third blocks, 85% of the tones were at 500 Hz (*standards*) and 15% of the tones were at 550 Hz (*deviants*). Tones occurred at a rate of  $\approx 2.5 \text{ Hz}$ . In the second block, the standards were replaced by silences (i.e., only deviant tones occurred.) Traditional event-related averages and time-frequency analyses revealed cortical responses between approximately 25 ms and 250 ms from tone onset. As expected from previous scalp EEG and animal studies, responses to standards were weak, responses to deviants were stronger, and responses to deviants only were strongest. For a detailed description of the traditional ECoG methods and results, see [17].

In the analysis that follows, we applied our synchronization measure  $T(\mathbf{x}[n, \eta]|\mathbf{y})$  to three electrodes from the second block of tones (deviants only) in which the evoked responses were strongest. For convenience, we refer to the three electrodes as *A*, *B*, and *C*. We considered times 125 ms preceding the stimulus onset to 220 ms following the stimulus onset, chose  $k'=40$  ensemble members, and set  $\sigma_D(\mathbf{x}'[n+\eta])$  in Eq. (12) to zero in what follows to obtain the most conservative measure. We did not average reference the data due to the small number (nine) of electrodes. Therefore, the shared reference electrode may artificially increase the synchronization results. If this effect were important, we would expect all electrode pairs to show strong synchronization for all time. We show below that the synchronization varies from strong to weak, and for some electrode pairs no synchronization was detected. Therefore, we assume that the reference electrode only weakly effects the synchronization results presented below.

In Fig. 7 we show the synchronization measure  $T(\mathbf{x}[n, \eta]|\mathbf{y})$  for electrodes *A* and *B*. The solid diagonal line denotes the location of zero time lag. The vertical and horizontal dashed lines denote the time of stimulus onset. From Fig. 7 it is clear that electrodes *A* and *B* are synchronous. We note that *A* and *B* become strongly synchronous approximately 90 ms after the stimulus onset and that the duration of the synchronization is longer in *A* than in *B*.

Next we show the synchronization between electrodes *C* and *A* in Fig. 8(a). It is clear that *C* and *A* are synchronous although less so than *A* and *B*. The synchronization is elongated in time along the *C* direction, and the maximum syn-

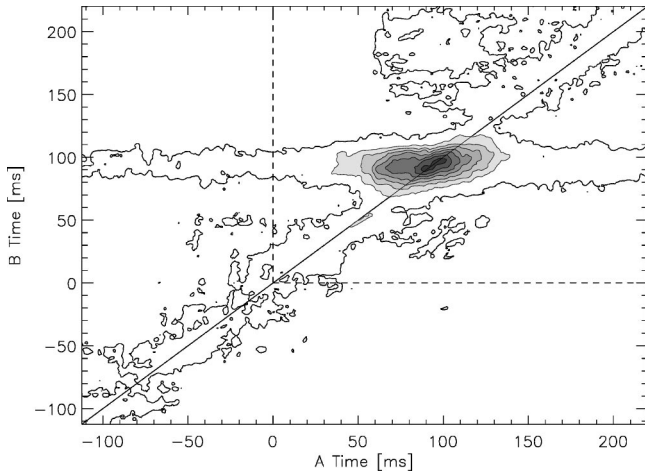


FIG. 7. The synchronization measure  $T(\mathbf{x}[n, \eta]|\mathbf{y})$  applied to electrodes  $A$  and  $B$  from the ECoG ERP experimental data.  $T(\mathbf{x}[n, \eta]|\mathbf{y})$  was smoothed over a two-dimensional window of size 11 at each time point. The solid diagonal line corresponds to the location of zero time lag. The horizontal and vertical dashed lines correspond to the time of stimulus onset. For this figure there are ten evenly spaced contour levels from 0.01 (white) to 0.19 (black). Note the region of strong synchronization from  $40 \text{ ms} < n < 130 \text{ ms}$  in  $A$  and  $60 \text{ ms} < n < 110 \text{ ms}$  in  $B$ .

chronization occurs after the stimulus, near 130 ms in  $C$  and 90 ms in  $A$ .

Finally in Fig. 8(b) we show the synchronization  $T(\mathbf{x}[n, \eta]|\mathbf{y})$  between electrodes  $C$  and  $B$ . In this case, the synchronization is very weak. Thus, electrodes  $A$  and  $B$  are strongly synchronous,  $C$  and  $A$  are weakly synchronous, and  $C$  and  $B$  are not significantly synchronous.

We can interpret these results in a qualitative manner consistent with the physiology of the human neocortex. That the synchronization follows the stimulus onset in Fig. 7 suggests the synchronization between electrodes  $A$  and  $B$  is induced by the stimulus. The area of maximum synchronization in Fig. 7 occurs at a physiologically reasonable temporal location, approximately 90 ms after the stimulus onset, and the closeness of the synchronization maximum to the diagonal suggests that electrodes  $A$  and  $B$  are synchronous with zero time lag. We may therefore make the hypothesis that the stimulus activates the cortical regions below electrodes  $A$  and  $B$  simultaneously. This suggests that a common input—perhaps from other cortical areas or deeper brain regions—activates both cortical regions simultaneously. In this way we can begin to map the cortical connectivity following a deviant auditory tone.

We present two more simulated examples to help interpret the synchronization results for electrodes  $C$ ,  $A$  and  $C$ ,  $B$ . We begin by noting that experimental ERPs are not precisely time locked to the stimulus onset. Different paths of action potential propagation, changing states of the subject, and inherent experimental error will vary the time at which the ERPs occur. Although the time interval between the stimulus and cortical response may vary, different cortical regions may still be strongly synchronous. In both simulated examples that follow,  $s^k[n]$  consists of an oscillatory burst 50 ms in duration and centered at  $n=175 \text{ ms}$ , while  $r^k[n]$  consists of an oscillatory burst 100 ms in duration, also centered at  $n=175 \text{ ms}$ . To each  $s^k[n]$  and  $r^k[n]$  we added sinusoidal noise such that the SNR=10.

To mimic the known variation in ERPs mentioned above, we consider two cases. In the first case, we include random time shifts (up to  $\pm 20 \text{ ms}$ ) in the location of the oscillatory bursts. We do this in such a way that, for each  $k$ , the pair of

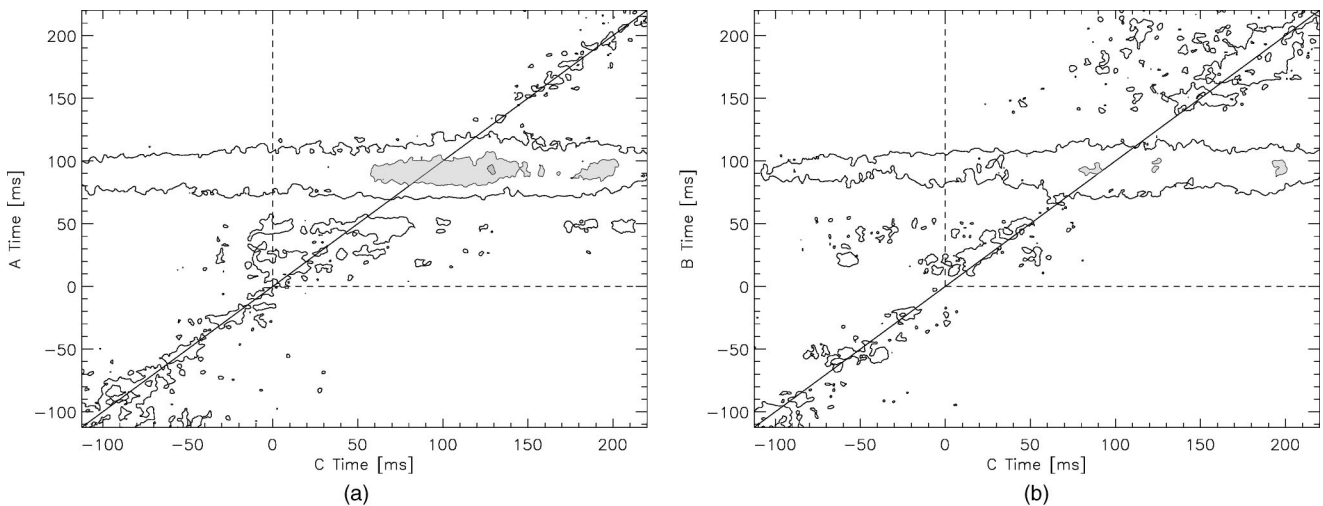


FIG. 8. The synchronization measure  $T(\mathbf{x}[n, \eta]|\mathbf{y})$  applied to electrodes from the ECoG ERP experimental data. In both figures,  $T(\mathbf{x}[n, \eta]|\mathbf{y})$  was smoothed over a two-dimensional window of size 11 at each time point. The solid diagonal line in both figures corresponds to the location of zero time lag. The horizontal and vertical dashed lines in both figures correspond to the time of stimulus onset. For both figures there are ten evenly spaced contour levels from 0.01 (white) to 0.19 (black). (a) The synchronization measure  $T(\mathbf{x}[n, \eta]|\mathbf{y})$  applied to electrodes  $C$  and  $A$  from the ECoG ERP experimental data. Note that the synchronization is elongated in  $C$  and is weaker than the synchronization between electrodes  $A$  and  $B$ . (b) The synchronization measure  $T(\mathbf{x}[n, \eta]|\mathbf{y})$  applied to electrodes  $C$  and  $B$  from the ECoG ERP experimental data. Note that the synchronization is weaker than the synchronization between the other electrode pairs.

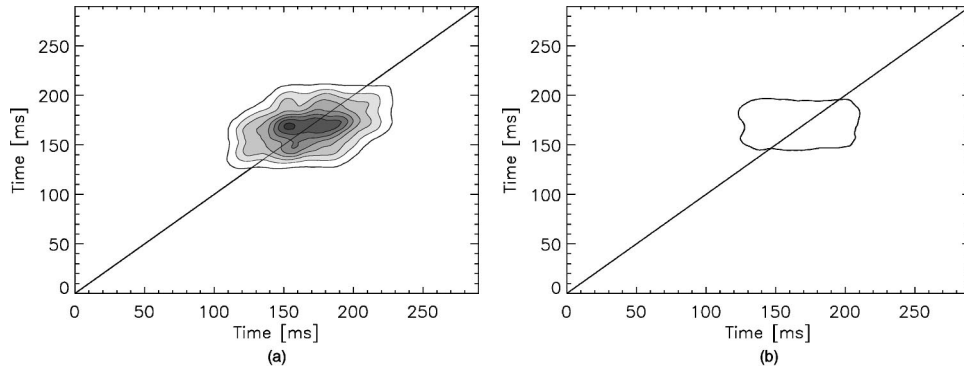


FIG. 9. The synchronization measure  $T(\mathbf{x}[n, \eta]|\mathbf{y})$  applied to shifted simulated data. In both figures,  $T(\mathbf{x}[n, \eta]|\mathbf{y})$  was smoothed over a two-dimensional window of size 11 at each time point. The solid diagonal line in both figures corresponds to the location of zero time lag. For both figures there are ten evenly spaced contour levels from 0.01 (white) to 0.19 (black). (a) The synchronization measure  $T(\mathbf{x}[n, \eta]|\mathbf{y})$  applied to uniformly shifted simulated data. The ensembles  $s$  and  $r$  consist of oscillatory bursts with the same center time. The oscillatory bursts in each ensemble member pair  $s^k[n]$  and  $r^k[n]$  are shifted in time by the same amount, up to  $\pm 20$  ms, and in the same direction. (b) The synchronization measure  $T(\mathbf{x}[n, \eta]|\mathbf{y})$  applied to randomly shifted simulated data. The ensembles  $s$  and  $r$  consist of oscillatory bursts with the same center time. The oscillatory bursts in each ensemble member pair  $s^k[n]$  and  $r^k[n]$  are shifted in time by different amounts, up to  $\pm 10$  ms, and in different directions.

ensemble members  $s^k[n]$  and  $r^k[n]$  are time shifted by the same amount and in the same direction. Thus, although the time series are not precisely time locked to the stimulus, they are precisely time locked to each other. We refer to this type of shifting as *uniform shifting*. In Fig. 9(a) we show the synchronization measure  $T(\mathbf{x}[n, \eta]|\mathbf{y})$  where  $\mathbf{x}^k[n]$  and  $\mathbf{y}^k[n]$  are the embeddings of  $s^k[n]$  and  $r^k[n]$ , respectively, and we have set  $\sigma_D(\mathbf{x}^k[n+\eta])$  in Eq. (12) to zero. We note that  $T(\mathbf{x}[n, \eta]|\mathbf{y})$  due to the uniformly shifted simulated data, shown in Fig. 9(a), is similar to the result for the experimental data shown in Figs. 7 and 8(a); both results possess an elongated region of synchronization centered near zero time shift.

For the second case of simulated data, the oscillatory bursts in the time series  $s^k[n]$  and  $r^k[n]$  are time shifted by random amounts (up to  $\pm 10$  ms.) But in this example, the time shifts for pairs of ensemble members  $s^k[n]$  and  $r^k[n]$  are not necessarily the same. Thus, the time series are neither time locked to the stimulus nor to each other. We refer to this type of shifting as *random shifting*. As above,  $\mathbf{x}^k[n]$  and  $\mathbf{y}^k[n]$  are the embeddings of  $s^k[n]$  and  $r^k[n]$ , respectively, and we have set  $\sigma_D(\mathbf{x}^k[n+\eta])$  in Eq. (12) to zero. The synchronization measure  $T(\mathbf{x}[n, \eta]|\mathbf{y})$  shown in Fig. 9(b) reveals very weak synchronization between the two randomly shifted ensembles. Here,  $T(\mathbf{x}[n, \eta]|\mathbf{y})$  allows one to draw the correct conclusion—if the two time series are neither time locked to the stimulus nor to each other, they are only weakly dependent. The two ensembles of time series are not independent because both time series respond to the stimulus at approximately the same time. This simulated result shown in Fig. 9(b) is consistent with the weak synchronization found between electrodes  $C$  and  $B$  and shown in Fig. 8(b).

The qualitative reasoning and simple simulations suggest the following conclusions. The strong synchronization between electrodes  $A$  and  $B$  may be due to simultaneous or uniformly shifted ERPs—this electrode pair may be driven

by a common source. The weak synchronization between electrodes  $C$  and  $B$  may be due to randomly shifted ERPs; although both electrodes respond to the stimulus, they do so in an unrelated way. Finally, the intermediate synchronization between electrodes  $C$  and  $A$  may be due to a combination of uniform shifting and small, random shifting. Thus, this electrode pair may be weakly driven by a common source.

## VI. CONCLUSIONS

In Sec. II we adapted the ensemble formalism to three current synchronization measures and introduced a synchronization measure  $T(\mathbf{x}[n, \eta]|\mathbf{y})$ . We showed in Sec. IV that  $T(\mathbf{x}[n, \eta]|\mathbf{y})$  is the most useful synchronization measure for the application of interest in the present work: analysis of data from electrode pairs in an ECoG ERP experiment. In Sec. V we applied  $T(\mathbf{x}[n, \eta]|\mathbf{y})$  to three electrode pairs from an ECoG ERP experiment and suggested relationships between the associated areas of cortex based on the similarity to measures of simulated data of uniformly shifted and randomly shifted responses.

We note that inferring cortical connectivity from the analysis of electrode recordings is a very difficult task. Unfortunately we cannot verify whether our synchronization (or any other) results for the experimental data correspond to physical connectivity in the cortex. Future experiments in which the cortical connectivity is known or can be determined independently could validate the relationship between synchronous electrodes and connected cortical regions.

## ACKNOWLEDGMENTS

The authors would like to thank members of the Knight Laboratory for useful discussions. M.A.K. was supported by the National Science Foundation.

- [1] P. L. Nunez, *Neocortical Dynamics and Human EEG Rhythms* (Oxford University Press, New York, 1995).
- [2] A. von Stein, C. Chaing, and P. Konig, *Proc. Natl. Acad. Sci. U.S.A.* **97**, 14 748 (2000).
- [3] P. L. Nunez, R. Srinivasan, A. Westdorp, E. Wijesinghe, D. M. Tucker, R. B. Silberstein, and P. Cadusch, *Electroencephalogr. Clin. Neurophysiol.* **103**, 499 (1997).
- [4] A. von Stein and J. Sarnthein, *Int. J. Psychophysiol.* **38**, 301 (2000).
- [5] A. Delorme and S. Makeig, *J. Neurosci. Methods* **134**, 9 (2004).
- [6] J. Arnhold, P. Grassberger, K. Lehnertz, and C. Elger, *Physica D* **134**, 419 (1999).
- [7] R. Quian Quiroga, J. Arnhold, and P. Grassberger, *Phys. Rev. E* **61**, 5142 (2000).
- [8] R. Quian Quiroga, A. Kraskov, T. Kreuz, and P. Grassberger, *Phys. Rev. E* **65**, 041903 (2002).
- [9] R. B. Duckrow and A. M. Albano, *Phys. Rev. E* **67**, 063901 (2003).
- [10] L. M. Pecora and T. L. Carroll, *Phys. Rev. Lett.* **64**, 821 (1990).
- [11] N. F. Rulkov, M. M. Sushchik, L. S. Tsimring, and H. D. I. Abarbanel, *Phys. Rev. E* **51**, 980 (1995).
- [12] M. G. Rosenblum, A. S. Pikovsky, and J. Kurths, *Phys. Rev. Lett.* **76**, 1804 (1996).
- [13] J. Bhattacharya, E. Pereda, and H. Petsche, *IEEE Trans. Syst. Man Cybern.* **33**, 85 (2003).
- [14] R. M. Gulrajani, *Bioelectricity and Biomagnetism* (Wiley, New York, 1998).
- [15] H. Abarbanel, R. Brown, J. Sidorowich, and L. Tsimring, *Rev. Mod. Phys.* **65**, 1331 (1993).
- [16] K. J. Friston, *Neuroimage* **5**, 213 (1997).
- [17] E. Edwards, M. Soltani, L. Y. Deouell, M. S. Berger, and R. T. Knight (unpublished).